RSC Advances

COMMUNICATION

View Article Online
View Journal | View Issue

Cite this: *RSC Adv.*, 2016, **6**, 48346

Mediator-free carbon nanotube yarn biofuel cell†

Cheong Hoon Kwon,‡[a] Young Bin Park,‡[a] Jae Ah Lee,[b] Young-Bong Choi,[c] Hyug-Han Kim,[c] Márcio D. Lima,[b] Ray H. Baughman[b] and Seon Jeong Kim*[a]

Received 11th March 2016
Accepted 9th May 2016

DOI: 10.1039/c6ra06570h

www.rsc.org/advances

Enzymatic biofuel cells are the most promising energy sources for implanted biomedical devices. However, direct implantation of biofuel cells has been limited by toxicity from metal-based redox mediators, and by a short operation time because of their instability, especially in physiological conditions. Here we introduce a yarn-type enzymatic biofuel cell for direct electron transfer using surface tension induced self-assembly of aligned multi-walled carbon nanotubes. This biofuel cell offers a maximum power density of 236 $\mu W\ cm^{-2}$, and an open circuit voltage of 0.61 V in 30 mM glucose-containing phosphate-buffered saline, without any mediators or chemical cross-linkers. Furthermore, the proposed self-assembled carbon nanotube-based structure provides enhanced stability for biofuel cells: 84% of the initial power output was consistently maintained after 20 days of continuous operation. Our biocompatible, microsized yarn biofuel cell electrode could be applied easily as needle or catheter shapes in various biomedical fields.

Biofuel cells (BFCs) are considered among the most appropriate candidates to replace existing energy sources used for implanted biomedical devices.[1,2] The concept of a BFC, which harvests electricity from glucose and oxygen, should enable continuous, biocompatible operation under physiological conditions. Previously reported BFC systems generally include a redox mediator to induce effective electro-communication between the enzyme and the electrode.[3,4] Although the redox mediator greatly helps electron transfer, it has some limitations, especially in biomedical applications. First, most redox mediators usually contain metal ions such as osmium, ruthenium and iron.[5] Even though such systems usually have very efficient electron transfer between the enzyme and the electrode surface leading to larger current outputs, the use of mediators in implantable devices could potentially generate issues of toxicity arising from the leakage of osmium complex.[6] Moreover, synthesizing redox mediators is very complicated, takes a long time, and requires many chemical treatments.[7] Based on these economic and toxic issues of redox mediators, mediator-free BFCs could serve as suitable systems for implantation.

Achieving electrical wiring between the enzyme and the electrode without a redox mediator, known as "direct electron transfer", is one of the main challenges for achieving a stable, biocompatible BFC.[8] Therefore, there have been many studies on ways to induce mediator-less enzymatic reactions associated with the materials of the electrode, enzymes, and techniques for entrapping enzymes in the electrode.[9–20] However, reported direct electron transfer systems still have some limitations. For example, they use promoters of electrochemical activity instead of a general redox mediator.[9–12] Their electrodes involve complicated chemical treatments for fabrication, especially using cross-linking or ionic liquids.[12–15] Furthermore, their sizes and shapes are difficult to be used for microsized devices.[17–20] They also have a short lifetime because of the instability of the electrode.[9–20]

Here, we successfully overcame the limitations of mediator-free BFCs for implantation with a simple and easy process using a self-assembled yarn electrode consisting of a multi-walled carbon nanotube (MWCNT) sheet, a conducting polymer, poly(3,4-ethylenedioxythiophene) (PEDOT),[21] and two enzymes. The MWCNT sheet was selected as the host material of our BFC based on its excellent electrical conductivity and vertically aligned structure.[22] These characteristics contribute to direct electron transfer between the enzyme and the MWCNT electrode. The electrons generated from the enzymatic reaction can be transferred easily through the yarn electrode because of shrinkage between the enzyme and MWCNTs caused by surface tension in the evaporating enzyme solution. In addition, this electrode structure can effectively entrap the enzyme by hydrophobic interactions between MWCNTs, and the stability of BFC

[a]*Center for Self-powered Actuation, Department of Biomedical Engineering, Hanyang University, Seoul 04763, Korea. E-mail: sjk@hanyang.ac.kr*

[b]*The Alan G. MacDiarmid NanoTech Institute, University of Texas at Dallas, Richardson, TX 75083, USA*

[c]*Department of Chemistry, Dankook University, Cheonan 31116, Korea*

† Electronic supplementary information (ESI) available. See DOI: 10.1039/c6ra06570h

‡ These authors contributed equally to this work.

has been enhanced accordingly. Our yarn-type BFC can be implanted with needles or catheters in a minimally invasive way, and is especially suitable for biomedical applications.

A three-layer MWCNT sheet[19] drawn from a spinnable forest of carbon nanotubes was prepared on a polytetrafluoroethylene (PTFE) supporter for maintaining the straightened plane shape in the solution. The rectangular, frame-like mold we used is illustrated in Fig. S1.† The conducting polymer, PEDOT, was coated on the MWCNT sheet. As shown in Fig. S1a,† after coating with the PEDOT polymer, the MWCNT sheet was fully immersed in the enzyme solution overnight. In enzyme solution, glucose oxidase (GOx) from *Aspergillus niger* was used as an anodic enzyme, and bilirubin oxidase (BOD) from *Myrothecium verrucaria* was used as a cathodic enzyme (characterization of enzyme kinetics and enzyme activities are additionally comprised in the "Materials and Method" of the ESI†). When the MWCNT sheet was separated from the enzyme solution and allowed to dry, surface tension induced self-assembly of the MWCNT yarn (Fig. S1b:† middle image). After a few hours of drying, the MWCNT yarn electrode was finally fabricated by additional shrinkage with water evaporation (Fig. S1b:† right image). During this shrinkage, the triangular promontories on the top and bottom of the PTFE supporter help the MWCNT sheet shrinking uniformly to the center from both sides. This scheme of self-assembled shrinkage is shown in Fig. 1a and S1† in detail. Here, PEDOT can play a fundamental role for enhancing the electrical conductivity and enzyme affinity of the MWCNT electrode. Although PEDOT can help the electrical wiring between MWCNT electrode and the enzyme,[3] the weight percentage of PEDOT on the MWCNT electrode should be carefully optimized for direct electron transfer and stability of BFC. We optimized the weight percentages of PEDOT and MWCNT sheet for anode current density measured by linear sweep voltammetry at 0 V and equivalent series resistance (ESR) measured using Nyquist plots, as shown in Fig. S2.† As a result, 2 wt% of PEDOT, relatively low concentration of PEDOT, was used for mediator-free BFC system in this study.

The surface and cross-sectional images of the BFC electrode are shown in scanning electron microscopy (SEM) images in Fig. 1b and c. Although we did not apply any external pressure or cross-linkers, the assembled yarn electrode has a vertically aligned and compressed yarn-type structure, as shown in Fig. 1b. A cross-sectional SEM image of the enzymatic electrode shows the corrugated multilayer structure of the enzyme and MWCNT (Fig. 1c). This corrugated structure offering spaces between MWCNTs can physically provide sufficient loading amount of each enzyme, 95 ± 1.8 wt% of GOx for the anode, and 98 ± 1.1 wt% of BOD for the cathode, respectively. We compared the surface images by SEM of the bare MWCNT yarn, the PEDOT/MWCNT yarn and the GOx enzyme-entrapped PEDOT/MWCNT yarn (Fig. S3†), for verifying the differences in dimensions produced by coating with the PEDOT conducting polymer, and loading of the enzyme as a guest on the bare MWCNT.

Enzymatic reactions based on direct electron transfer were achieved with this shrinkage induced by surface tension. During this process, as the water contained in the enzyme

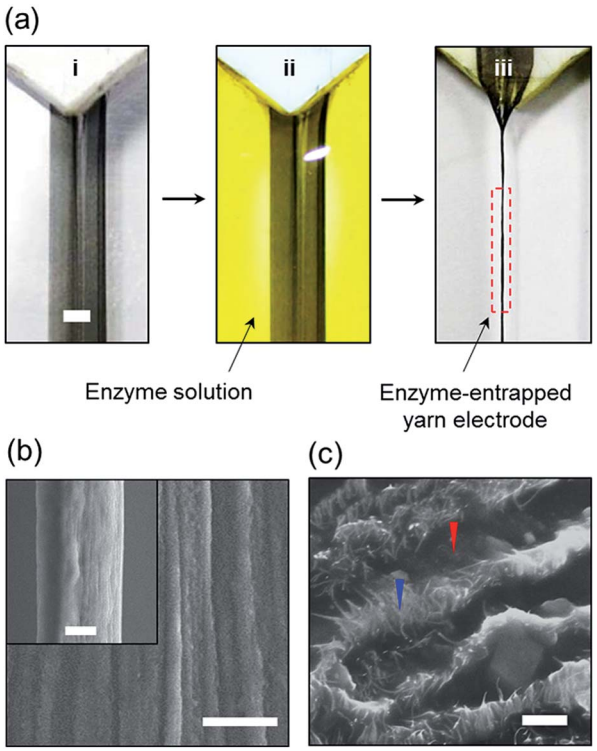

Fig. 1 Schematic representation of enzyme-loaded MWCNT self-assembled yarn biofuel cell electrodes. (a) Self-assembly with collapse of the MWCNT yarn carrying enzyme by surface tension. Scale bar = 2 mm. (i) PEDOT-coated MWCNT sheet on the PTFE mold (ii) MWCNT sheet immersed in enzyme solution (iii) Shrinkage of the MWCNT sheet to form an enzyme-entrapped yarn electrode after being removed from enzyme solution and dried for a few hours. The red dotted region of the yarn was finally used for electrochemical testing of the BFC. (b) SEM images showing surfaces of the yarn electrode. Scale bar = 5 μm; inset = 10 μm. The diameter of the yarn electrode is 28 μm. (c) Cross-sectional image of the yarn electrode. The blue arrowhead indicates the MWCNT layer, and the red arrowhead indicates the enzyme entrapped between layers. Scale bar = 2 μm.

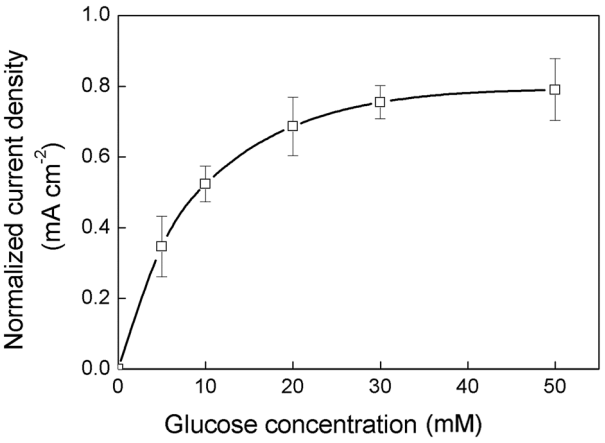

Fig. 2 Normalized anodic current density depending on the glucose concentrations from 0 to 50 mM. The error bars show the s.d. from the mean value of current densities for three independent experiments.

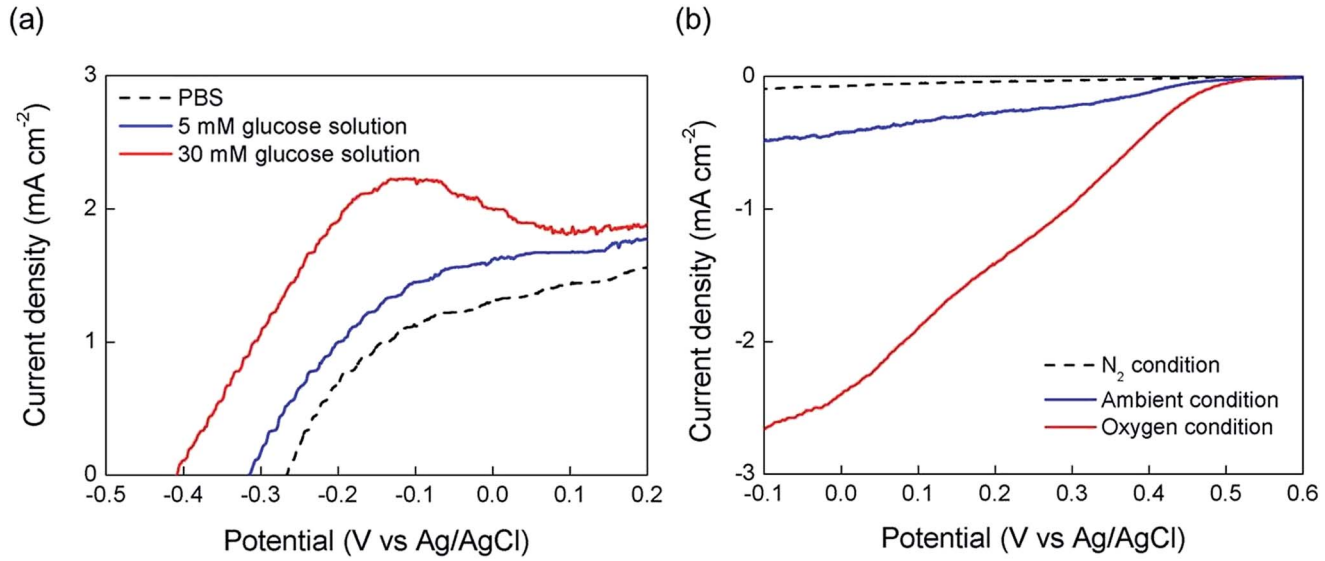

Fig. 3 Half-cell performance of a MWCNT-anode with GOx and a cathode with BOD. (a) Polarization curve of the anode in the PBS buffer solution not containing glucose (black dotted line), in 5 mM glucose in PBS (blue solid line), and in 30 mM glucose solution (red solid line). (b) Polarization curve of the cathode in N_2-saturated (black dotted line), ambient (blue solid line), and oxygen-saturated conditions (red solid line).

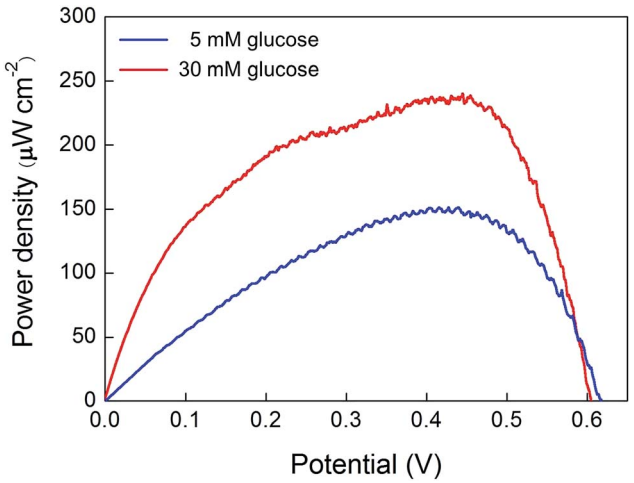

Fig. 4 BFC performance of depending on the power density in 5 mM glucose in an ambient condition (blue solid line) and 30 mM glucose in the oxygen-saturated condition (red solid line).

solution is extracted uniformly, the surface tension acts to compress the electrode. This shrunken electrode can provide enhanced electrical communication between the enzyme and the MWCNT. We measured the performances of the anode and cathode electrodes by observing the redox peaks using cyclic voltammetry. The current density measured in this way was normalized to the yarn's lateral surface area calculated from the yarn electrode diameter as measured by SEM.

To verify direct electron transfer in the anodic reaction, we measured the current density while changing the glucose concentration. Anodic current density according to the glucose concentration from 0 to 50 mM was saturated at 30 mM glucose, and it was attributed by an inherent Michaelis–Menten type feature of the enzymatic reaction (Fig. 2). As shown in Fig. 3a, we found that the anodic reaction started from −0.41 V (onset potential) at 30 mM glucose, to −0.31 V *versus* Ag/AgCl at 5 mM glucose. We obtained a current density of 330 μA cm^{-2} in 5 mM glucose, and 700 μA cm^{-2} in 30 mM glucose after normalizing against the current density value of glucose-free conditions which already reflects the influence of the metallic impurities within the electrode such as PEDOT oxidant. Furthermore, the reaction peak of the anode was observed at around −0.1 V. With increasing glucose concentrations, the current density increased sharply to 30 mM. As shown in Fig. 3b, the current density showed significant increases when the fuel (oxygen) was added. We obtained a current density of 350 μA cm^{-2} in the ambient state, and 2.33 mA cm^{-2} at 0 V in the oxygen-saturated condition, also after normalization against the nitrogen-saturated condition. This sharp increase in current density means that electrons could be transferred effectively through the electrode. It is known that the distance between the electrode and the active site of the enzyme is one of the most important factors to be considered for such actions.[6] In addition, the closest distance between the carbon electrode and the T1 active site of BOD is less than 10 Å.[23] This electron transfer distance provides an accessible distance for inducing direct electron transfer in our compressed carbon nanotube structure. Therefore, electrons can be transferred effectively in the BOD-cathodic electrode. The cyclic voltammetry results on the wide potential range from −0.6 V to 0.6 V for the anode, and from −0.4 V to 0.8 V for the cathode, as shown in Fig. S4.†

Performance of the completed BFC system was measured by cyclic voltammetry of the two-electrode system without a separating membrane. The power density was measured at 30 mM glucose in oxygen-saturated phosphate-buffered saline (PBS), and at 5 mM glucose under ambient conditions. As shown in Fig. 4, the maximum power density at 5 mM glucose was 150 μW

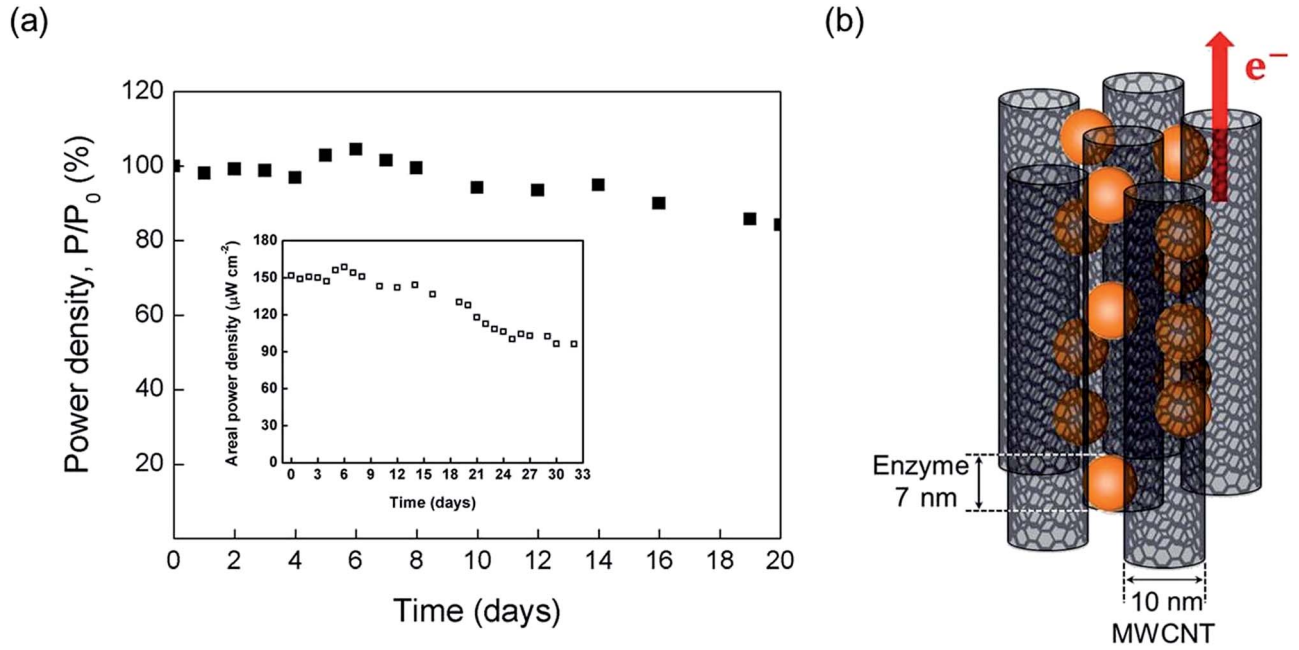

Fig. 5 Stability of the final BFC system. (a) Normalized power (P/P_0, %) for 20 days with continuous operation under quiescent condition. Experiments were carried out in PBS (0.1 M, pH 7.0 at 37 °C), and a 5 mV s^{-1} scan rate. Inset: power density output for 32 days. (b) Schematic diagram of enzyme entrapment and the direct electron transfer pathway in the vertically aligned MWCNT.

Table 1 Comparison of direct electron transfer-based glucose/O_2 biofuel cells

Bioelements (anode/cathode)	Solution	Stability (h)	Power (μW cm^{-2})	Type of electrode	Ref.
CDH[a]/laccase	Citrate buffer pH 4.5, 5 mM glucose	>38[c]	>5	Rod	15
CDH[a]/BOD	PBS pH 7.4, 5 mM glucose	>6[c]	3	Rod	16
CDH[a]/BOD	PBS pH 7.4, 5 mM glucose	>30[c]	3.2	Disk	17
GOx/laccase	PBS pH 7.0, 50 mM glucose	~2.7[c,d]	1300	Disk	14
GDH[b]/BOD	100 mM citrate buffer and 1 mM $CaCl_2$, 10 mM glucose	>72[e]	122	Film	10
GOx/BOD	PBS pH 7.4, 30 mM glucose	768[f]	236	Yarn	This work

[a] Cellobiose dehydrogenase. [b] Glucose dehydrogenase. [c] 50% of initial power. [d] Recalculated from OCV drop. [e] 90% of initial power. [f] 63% of initial power, 84% of initial power after 480 hours.

cm^{-2} under the ambient condition, and 236 μW cm^{-2} in 30 mM glucose at 0.45 V under an oxygen-saturated condition. The open circuit voltage was ~0.61 V in both conditions. In addition, the electrical resistance of the full system was analyzed with ESR values measured at 1 kHz. The resistance of the full system was 883 Ω; 333 Ω for the cathode, and 407 Ω for the anode (Fig. S5†). The electronic diffusion coefficient was estimated from the slope of the peak currents according to the square root of scan rates in Fig. S6.† Compared to the BFC electrode without enzymatic reaction, the diffusion coefficient of BFC electrode was doubled with enzymatic reaction. It was confirmed that the direct electron transfer between the enzyme and the electrode clearly occurs.

The stability of the complete system was measured under 5 mM glucose in PBS in ambient conditions for 32 days by cyclic voltammetry. Our system maintained 84.2% of its initial power for 20 days, and 63.3% after 32 days (Fig. 5a). Furthermore, this stability was remarkably enhanced even though we did not apply any cross-linking treatments for preventing the leakage of entrapped enzyme in the electrode. We think that this improvement is fundamentally based on the hydrophobicity of the MWCNT electrode. Essentially, hydrophobic interactions in this electrode maintain the compressed structure in the hydrophilic liquid.[22] The entrapped enzymes can be closely oriented between carbon nanotubes (as illustrated in Fig. 5b). It effectively prevents any leakage of the enzyme, so that the stability of the BFC is enhanced compared with the previously reported existing mediator-less biofuel cells especially, for glucose/O_2 BFCs (Table 1).

Conclusions

We have demonstrated a newly developed microsized GOx/BOD carbon nanotube yarn BFC produced by self-assembly. This has

two important features. First, the mediator-free BFC electrodes were introduced successfully by a simple shrinkage process, without using any complicated procedures or metal-based mediators. Second, stability was improved because of the effective electrical wiring of the BFC system with hydrophobic interactions between carbon nanotubes. This can effectively prevent leakage of the enzyme from the BFC electrodes. This unique yarn-type electrode provides possibilities for micro-electrical devices with several advantages for implantation in biomedical fields, because it does not contain any harmful materials such as osmium-based redox mediators, and has long-term stability for implantation. This microsized, biocompatible yarn biofuel cell could be applied to animal/human body implantation, and to a variety of biomedical electrical devices, such as pacemakers, neurostimulators, and drug delivery systems.

Acknowledgements

This work was supported by the Creative Research Initiative Center for Self-powered Actuation and the Korea-US Air Force Cooperation Program Grant No. 2013K1A3A1A32035592 in Korea. Support at the University of Texas at Dallas was provided by Air Force Office of Scientific Research grants FA9550-15-1-0089 and AOARD-FA2386-13-4119, NASA grants NNX14CS09P and NNX15CS05C, and the Robert A. Welch Foundation grant AT-0029.

Notes and references

1 A. Heller, *Phys. Chem. Chem. Phys.*, 2004, **6**, 209–216.
2 I. Ivanov, T. Vidaković-Koch and K. Sundmacher, *Energies*, 2010, **3**, 803–846.
3 C. H. Kwon, S. H. Lee, Y. B. Choi, J. A. Lee, S. H. Kim, H. H. Kim, G. M. Spinks, G. G. Wallace, M. D. Lima, M. E. Kozlov, R. H. Baughman and S. J. Kim, *Nat. Commun.*, 2014, **5**, 3928.
4 A. Ramanavicius, A. Kausaite-Minkstimiene, I. Morkvenaite-Vilkonciene, P. Genys, R. Mikhailova, T. Semashko, J. Voronovic and A. Ramanaviciene, *Chem. Eng. J.*, 2015, **264**, 165–173.
5 F. P. Cardoso, S. Aquino Neto, L. B. Crepaldi, S. Nikolau, V. P. Barros and A. R. De Andrade, *J. Electrochem. Soc.*, 2014, **161**, 445–450.
6 M. Falk, Z. Blum and S. Shleev, *Electrochim. Acta*, 2012, **82**, 191–202.
7 Z. Gao, G. Binyamin, H. H. Kim, S. C. Barton, Y. Zhang and A. Heller, *Angew. Chem., Int. Ed.*, 2002, **114**, 838–841.
8 M. Falk, C. W. Narváez Villarrubia, S. Babanova, P. Atanassov and S. Shleev, *ChemPhysChem*, 2013, **14**, 2045–2058.
9 V. Jouikov and J. Simonet, *ECS Trans.*, 2013, **45**, 1–8.
10 C. X. Guo and C. M. Li, *Phys. Chem. Chem. Phys.*, 2010, **12**, 12153–12159.
11 V. Scherbahn, M. T. Putze, B. Dietzel, T. Heinlein, J. J. Schneider and F. Lisdat, *Biosens. Bioelectron.*, 2014, **61**, 631–638.
12 O. Yehezkeli, R. Tel-Vered, S. Raichlin and I. Willner, *ACS Nano*, 2011, **5**, 2385–2391.
13 X. Wu, F. Zhao, J. R. Varcoe, A. E. Thumser, C. Avignone-Rossa and R. C. Slade, *Biosens. Bioelectron.*, 2009, **25**, 326–331.
14 K. Stolarczyk, D. Łyp, K. Żelechowska, J. F. Biernat, J. Rogalski and R. Bilewicz, *J. Power Sources*, 2014, **249**, 263–269.
15 K. Stolarczyk, D. Łyp, K. Zelechowska, J. F. Biernat, J. Rogalski and R. Bilewicz, *Electrochim. Acta*, 2012, **79**, 74–81.
16 T. Miyake, S. Yoshino, T. Yamada, K. Hata and M. Nishizawa, *J. Am. Chem. Soc.*, 2011, **133**, 5129–5134.
17 A. Zebda, C. Gondran, A. Le Goff, M. Holzinger, P. Cinquin and S. Cosnier, *Nat. Commun.*, 2011, **2**, 370.
18 V. Coman, C. Vaz-Dominguez, R. Ludwig, W. Harreither, D. Haltrich, A. L. De Lacey, T. Ruzgas, L. Gorton and S. Shleev, *Phys. Chem. Chem. Phys.*, 2008, **10**, 6093–6096.
19 V. Coman, R. Ludwig, W. Harreither, D. Haltrich, L. Gorton, T. Ruzgas and S. Shleev, *Fuel Cells*, 2010, **10**, 9–16.
20 X. Wang, M. Falk, R. Ortiz, H. Matsumurad, J. Bobacka, R. Ludwig, M. Bergelin, L. Gorton and S. Shleev, *Biosens. Bioelectron.*, 2012, **31**, 219–225.
21 J. A. Lee, M. K. Shin, S. H. Kim, S. J. Kim, G. M. Spinks, G. G. Wallace, R. Ovalle-Robles, M. D. Lima, M. E. Kozlov and R. H. Baughman, *ACS Nano*, 2012, **6**, 327–334.
22 M. Zhang, S. Fang, A. A. Zakhidov, S. B. Lee, A. E. Aliev, C. D. Williams, K. R. Atkinson and R. H. Baughman, *Science*, 2005, **309**, 1215–1219.
23 P. Ramírez, N. Mano, R. Andreu, T. Ruzgas, A. Heller, L. Gorton and S. Shleev, *Biochim. Biophys. Acta*, 2008, **1777**, 1364–1369.

